

# A Highly Efficient 1-bit Reflectarray Antenna Using Electromagnet-Controlled Elements

Ao Hu<sup>ID</sup>, *Graduate Student Member, IEEE*, Keisuke Konno<sup>ID</sup>, *Member, IEEE*,  
Qiang Chen<sup>ID</sup>, *Senior Member, IEEE*, and Toru Takahashi<sup>ID</sup>, *Senior Member, IEEE*

**Abstract**—A novel mechanically reconfigurable reflectarray element actuated by an electromagnet working in C-band is proposed. The 1-bit phase shift of reflecting wave is achieved by bending a half-wavelength dipole with magnetostatic force. Due to the isolation between element and RF phase shifter, the proposed reflectarray element is free from insertion loss. This is the first article demonstrating the performance of a reconfigurable reflectarray with the element totally isolated from the RF phase shifter. Due to the contactless reconfigurable system, the mechanical connection between the electromagnet and the reflectarray element is physically unnecessary. Prototypes of the proposed reconfigurable reflectarray elements are fabricated and their mechanical tunability is theoretically and experimentally clarified. The detailed working principle of electromagnet control and implementation method are discussed. Next, a  $25 \times 8$  1-bit reconfigurable reflectarray using the proposed elements is fabricated and its scattering performance is demonstrated via field measurement. The measured gain and aperture efficiency of the fabricated 1-bit reconfigurable reflectarray are 22.7 dBi and 34.0% at specular direction, respectively. According to a comparison with previous works, it is clarified that the aperture efficiency of the proposed 1-bit reconfigurable reflectarray outperforms previously developed ones.

**Index Terms**—Electromagnets, magnetostatics, ON-OFF control, reconfigurable antennas, reflectarrays.

## I. INTRODUCTION

A REFLECTARRAY (RA) is well known as one of the promising antennas. The RA is a kind of reflector antenna, and its reflecting surface is composed of a number of array elements illuminated by a primary source such as a horn antenna. The reflecting surface is designed so that its main beam is directed in a specific direction. Starting from the first RA that has been proposed as an array of bulky waveguides,

extensive efforts have been dedicated to the development of various RAs [1]. For example, studies on planar RA [2], [3], [4], [5], [6], multilayered RA [7], [8], 3-D-printed RA [9], [10], [11], [12], and combination of RA and phased arrays [13], [14] have been reported so far.

According to the recent advancement of wireless technologies toward high-frequency band such as millimeter waves, the so-called reconfigurable RA has been studied. The reconfigurable RA is capable of controlling their main-beam direction and high propagation loss at the high-frequency band can be compensated. According to their mechanism of reconfigurability, the reconfigurable RA is roughly categorized into electrically reconfigurable RA and mechanically reconfigurable RA.

The electronically reconfigurable RA has been developed so far and their main-beam direction is controlled using RF phase shifters such as p-i-n diodes or varactor diodes. RA antennas with  $160 \times 160$  elements have been proposed [15]. The 1-bit phase shifters using p-i-n diodes are loaded with the RA elements and beam scanning capability of the RA has been demonstrated. A wideband 1-bit reconfigurable RA antenna also using p-i-n diodes, which has a relatively higher aperture efficiency, has been reported [16]. A wideband RA based on single-layer magnetolectric dipole elements with 1-bit reconfigurability has been proposed [17]. An aperture-coupled patch element with a varactor diode has been proposed and applied to electronically reconfigurable RA [18], [19]. A couple of electronically reconfigurable RA elements for dual-linearly polarized RA or multipolarization RA have been proposed [20], [21], [22]. A circularly polarized 1-bit reconfigurable RA based on p-i-n diode to change element rotation angle electromagnetically has been presented [23]. A 1-bit time-modulated method in reconfigurable-intelligent-surface (IRS) applications has also been demonstrated [24]. The major advantages of the electronically reconfigurable RA are high-speed and reliable beam scanning, while their major disadvantages are high insertion loss and nonlinearity of diodes. Although micro-electromechanical systems (MEMS) and liquid crystal (LC) are also known as promising technologies for reconfigurable systems, it has been indicated that their major disadvantages are high loss at microwave or millimeter-wave frequency bands [25], [26].

On the other hand, to overcome the insertion loss of p-i-n diodes and other electronic switches, the mechanically reconfigurable RA has been developed as counterparts of

Manuscript received 3 June 2023; revised 13 September 2023; accepted 7 October 2023. Date of publication 19 October 2023; date of current version 9 February 2024. This work was supported in part by the Doctoral Program for World-Leading Innovative and Smart Education (WISE Program) for Artificial Intelligence and Electronics of Tohoku University and in part by the Japan Society for the Promotion of Science (JSPS) KAKENHI under Grant 22K04061. (Corresponding authors: Ao Hu; Keisuke Konno.)

Ao Hu, Keisuke Konno, and Qiang Chen are with the Department of Communications Engineering, Graduate School of Engineering, Tohoku University, Sendai 980-8577, Japan (e-mail: hu.ao.p7@dc.tohoku.ac.jp; keisuke.konno.b5@tohoku.ac.jp).

Toru Takahashi is with the Antennas Technology Department, Information Technology Research and Development Center, Mitsubishi Electric Corporation, Kamakura 247-8520, Japan.

Color versions of one or more figures in this article are available at <https://doi.org/10.1109/TAP.2023.3324457>.

Digital Object Identifier 10.1109/TAP.2023.3324457

0018-926X © 2023 IEEE. Personal use is permitted, but republication/redistribution requires IEEE permission.  
See <https://www.ieee.org/publications/rights/index.html> for more information.

electronically reconfigurable RA [27], [28], [29]. The main-beam direction of the mechanically reconfigurable RA antennas is controlled using mechanical phase shifters such as actuators. Mechanically reconfigurable RA using rotational elements or slotted patches of tunable height has been proposed [30], [31], [32]. RA elements are mechanically connected with actuators under the ground plane and their rotation angle or height can be controlled by the actuators so that the main beam of the RA is directed to a specific direction. In recent years, a couple of new approaches for beam scanning of mechanically reconfigurable RA have been proposed, e.g., rotation of a feed antenna [33] or rotation of RA itself [34]. Major advantages of the mechanically reconfigurable RA are continuous phase variation and high-power handling capability, while their major disadvantages are slower scanning speed and complicated physical connection system.

It should be indicated that a couple of disadvantages of the electronically/mechanically reconfigurable RA stems from both the RF coupling and the mechanical connection between RA elements and RF phase shifters. For example, as mentioned earlier, the electronically reconfigurable RA suffers from high insertion loss and nonlinearity of diodes because RA elements are electromagnetically coupled with diodes at the RF frequency band. On the other hand, relatively high isolation between RA elements and RF phase shifters (i.e., actuators) can be kept at the RF frequency band for the mechanically reconfigurable RA, but the complicated mechanical connection between them is necessary. As a result, the fabrication of the mechanically reconfigurable RA is cumbersome. As mentioned above, electrical or mechanical contact between RF phase shifters and RA elements often results in problems such as high loss or fabrication difficulty. To the best of authors' knowledge, a reconfigurable RA element based on electronically/mechanically contactless RF phase shifters has not been proposed.

In this article, a mechanically contactless reconfigurable RA element using electromagnets is proposed. The proposed reconfigurable RA elements are composed of metallic dipole over flexible supporting structures backed by a ground plane. Metallic dipole elements are attached with magnetic materials such as steel and their height is tunable by static magnetic field generated by electromagnets behind the ground plane. The static magnetic field can penetrate the ground plane, whereas the electromagnets themselves are isolated from the RF signals, including incident/reflection waves by the ground plane. Because the electromagnets (i.e., phase shifters) are electrically decoupled with the RA elements in the RF frequency band, the proposed RA elements are free from insertion loss of the phase shifters. Mechanical/RF connection between RA elements and RF phase shifters, soldering of diodes, and complicated mechanical fabrication is unnecessary for the proposed reconfigurable RA element. As a result, the proposed RA demonstrates relatively higher aperture efficiency performance than previously developed 1-bit reconfigurable RAs.

This article is organized as follows. In Section II, an electromagnet-controlled RA element is proposed and designed. Next, prototypes of the electromagnet-controlled RA

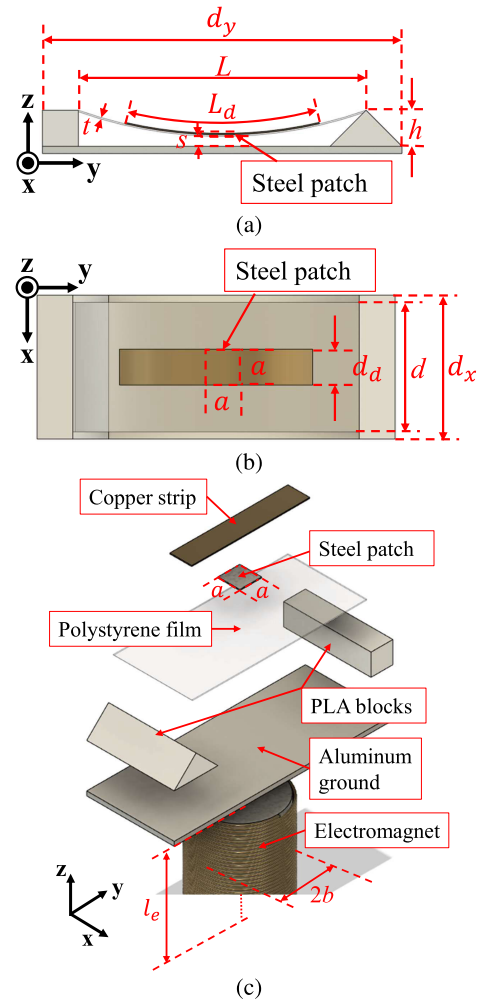


Fig. 1. Demonstration of electromagnet-controlled RA element: (a) side view, (b) top view, and (c) bird's eye view.

element are fabricated and their mechanical reconfigurability using electromagnets is measured. In Section III, a 1-bit  $25 \times 8$  RA antenna is fabricated, and its systematic design methods were introduced. In Section IV, the scattering performance of the fabricated prototype is measured in the outdoor environment and the measured results are discussed. Finally, Section V concludes this work.

## II. DESIGN AND VALIDATION OF RA ELEMENT USING ELECTROMAGNET

### A. Design and Working Principle of the RA Element

The configuration of the proposed electromagnet-controlled RA element is shown in Fig. 1. On the top of the geometry, there is a flexible copper strip with length and width of  $L_d$  and  $d_d$ . A small square steel patch of width  $a$  is underneath the center of the copper strip. In this article,  $a = d_d$  is kept throughout the study. The height of the steel patch over the ground is  $s$ . A flexible film with thickness  $t$ , length  $L$ , and width  $d$  is attached below the steel patch. The small steel patch is sandwiched between the copper strip and the film. The film is the supporting substrate for the copper strip, and it is taped on the film. Both the film and the copper strip are

flexible so that they can be bent simultaneously when a static magnetic field is applied to the steel patch. The film is made of elastic polystyrene with relative permittivity  $\epsilon_r = 2.6$  and loss tangent  $\tan\delta = 0.007$ . A rectangular block and a right-angle trigon block that are made of 15% infilled polylactic acid (PLA) ( $\epsilon_r = 1.25$  and  $\tan\delta = 0.01$ ) are placed below the film. The two blocks with height  $h$  are supporting structures for the upper components. The rectangular block clamps to the polystyrene on one end. The flat top surface of the rectangular block can flatten the polystyrene film when the magnetostatic force is not applied. On the other end, the right-angle trigon block supports the polystyrene film at the same height. The trigon shape helps the polystyrene film to slip on the other end with small mechanical resistance when the magnetostatic force is applied. An aluminum ground with length  $d_y$  and width  $d_x$  is attached to the bottom of the blocks. Underneath the ground, a cylindrical dc-controlled electromagnet with radius  $b$  and length  $l_e$  is attached.

The phase tuning mechanism is based on the height-tunable resonator approach [35]. The flexible copper strip over the elastic polystyrene film is flat when the electromagnet turns off, which forms a straight half-wavelength dipole over ground plane. Once the electromagnet turns on, the square steel patch underneath the center of the copper strip is attracted to the ground plane by the magnetostatic force, which then forms a bent dipole over ground plane. Such deformation and height tunability of the dipole element result in the difference of electromagnetic response, i.e., phase of reflection coefficient [32]. Simulation results in Section II-B demonstrate the difference in electromagnetic response between straight/bent dipole elements. The attracting force is generated from magnetic coupling between the electromagnets and the steel patch via static magnetic field penetrating the ground plane. Although the magnetostatic field penetrates the ground plane, RF signals are shielded by the ground plane. Therefore, complete RF isolation between the RA element and the electromagnet (i.e., RF phase shifter) is achievable by the proposed RA element. As a result, the proposed RA element is free of insertion loss of the RF phase shifter.

### B. Scattering Performance Analysis

Scattering performance of the electromagnet-controlled RA element under 2-D periodic boundary condition (PBC) is simulated by method of moments (MoM) using commercial simulator software FEKO. The working frequency of the proposed electromagnet-controlled RA element is 4.4 GHz. The array spacing is  $d_x = 20$  mm ( $0.293\lambda$ ) and  $d_y = 50$  mm ( $0.733\lambda$ ). Dimensions of the RA element here are optimized ones according to the mechanical performance analysis shown in Section II-C. Variation of reflection coefficient with respect to height  $s$  is shown in Fig. 2. It is found that  $180^\circ$  phase shift is available for two different angles of incidence  $(\theta_f, \varphi_f) = (0, 0^\circ), (30^\circ, 0^\circ)$  as  $s$  varies from 0 to 5 mm. Also, it is found that the drop of the magnitude is below 0.1 dB within the tunable range. The drop of the reflection magnitude stems from lossy dielectric material. According to the numerical results,

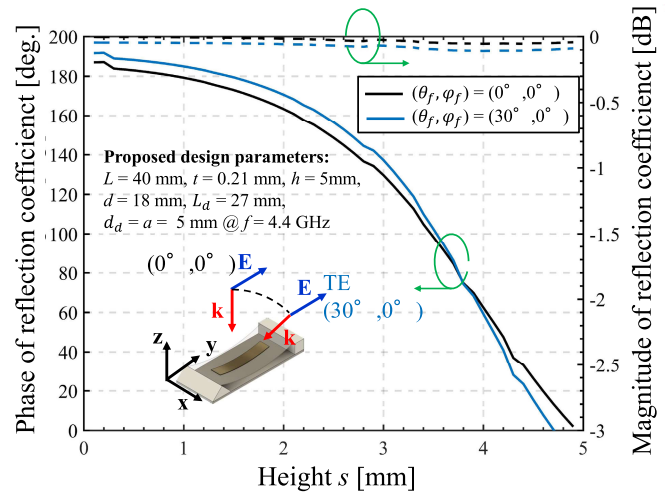


Fig. 2. Tunability of reflection coefficient with respect to height  $s$ .

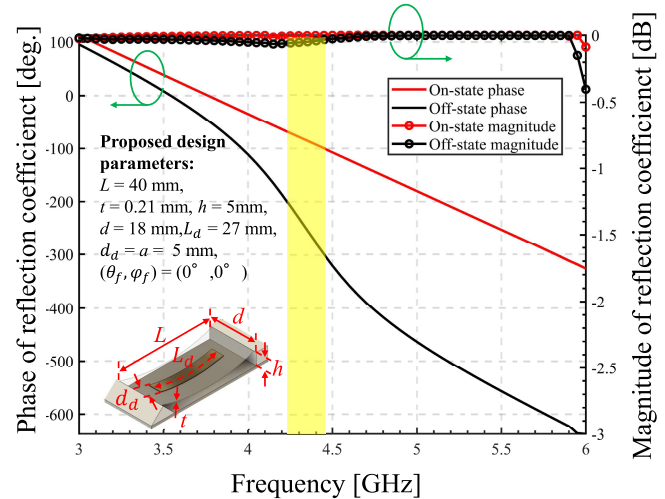


Fig. 3. Frequency response of reflection coefficient (yellow zone represents bandwidth where the phase difference between ON-state and OFF-state is ranging from  $160^\circ$  to  $200^\circ$ ).

it can be concluded that the proposed RA element meets the requirements of composing 1-bit reconfigurable RA.

Fig. 3 shows the frequency response of the reflection coefficient. Here, the ON-state means that the electromagnet turns on, after which the steel patch is attracted to the ground plane and RA element is bent. Similarly, the OFF-state means that the electromagnet turns off, and then, the RA element keeps flatness. The switching process of ON-state and OFF-state forms the 1-bit configuration of element. As indicated in yellow zone (approximately from 4.25 to 4.45 GHz) in Fig. 3, the phase shift between ON-state and OFF-state is ranging from  $160^\circ$  to  $200^\circ$ . Meanwhile, it is found that the drop of the magnitude is at most 0.4 dB within the frequency band. According to the numerical results, it can be concluded that the proposed RA element keeps a phase shift of  $180^\circ$  within a specific frequency band without significant loss.

These simulation results demonstrate that the proposed electromagnet-controlled RA element is capable to reconfigure the phase of reflection coefficient between ON- and OFF-state without significant loss.

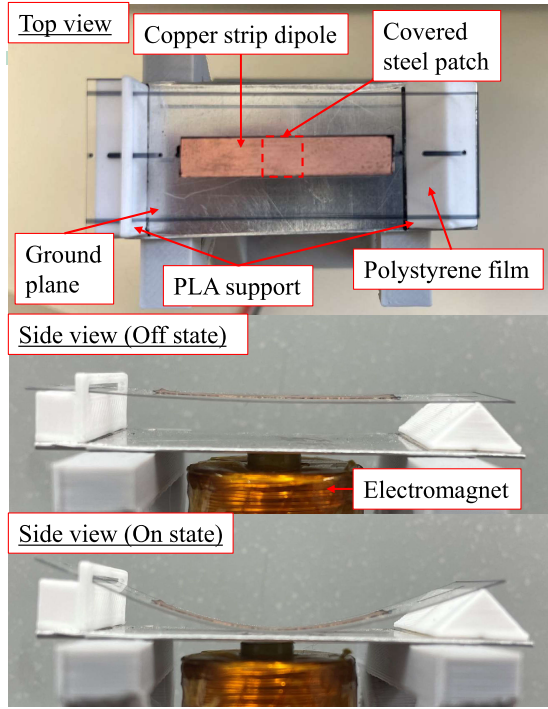


Fig. 4. Fabricated electromagnet-controlled RA element prototype (top view and side view) with electromagnet underneath ground plane connecting to dc power source.

### C. Mechanical Performance Analysis

To validate the height tunability of the proposed RA element, a mechanical study on polystyrene film deformation by imposing the magnetostatic force is performed. A formula for expressing attraction on a square piece of magnetic material with a square width of  $a$  in the uniform magnetic field is used to predict the magnitude of magnetostatic force  $F$  attracting the small steel patch [37]

$$\mathbf{F} = -\frac{|\mathbf{B}|^2 a^2}{2\mu_0} \hat{\mathbf{z}} \quad (1)$$

where  $a^2$  is the area of the square steel patch,  $\mu_0$  is the permeability of free space, and  $\mathbf{B}$  is the magnetic flux density at the steel patch. Since the magnetic flux density  $\mathbf{B}$  is generated by an electromagnet of finite solenoid coil style,  $\mathbf{B}$  can be assumed as

$$\mathbf{B} = -\frac{\mu_0 \mu_r n I}{2} \left\{ \frac{l_e + s + t_g}{\sqrt{b^2 + (l_e + s + t_g)^2}} - \frac{s + t_g}{\sqrt{b^2 + (s + t_g)^2}} \right\} \hat{\mathbf{z}} \quad (2)$$

where  $\mu_r$  is the relative permeability of the electromagnet iron core,  $n$  is the number of turns,  $I$  is the current flowing through the coil,  $s$  is the height of the steel patch, and  $b$  and  $l_e$  are the radius and length of the electromagnet, respectively. In this article, TMB-2006T is used as an electromagnet and the following parameters are substituted into (1) and (2):  $b = 10$  mm,  $l_e = 80$  mm,  $n = 4000$ , and  $\mu_r = 1000$  [36].

From the mechanics aspect of view, the deformation of polystyrene film can be modeled as a cantilever with clamped edges and a concentrated force  $F$  applying at its geometry

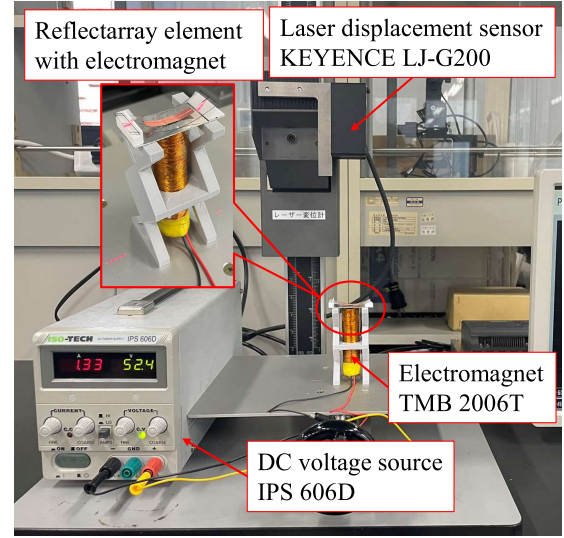


Fig. 5. Measurement system for height tunability of the electromagnet-controlled RA element prototype.

center. Thus, the height of the small steel patch attaching to the electromagnet-controlled element can be described using the following formula [38]:

$$\begin{aligned} s &= h + t - \delta \\ &= h + t - \frac{|\mathbf{F}|L^3}{4Edt^3} \end{aligned} \quad (3)$$

where  $t$  is the thickness of the polystyrene film and  $t_g = 1$  mm is the thickness of aluminum ground. The term  $\delta$  represents the displacement of the steel patch in the  $z$ -direction, which is further expressed by several terms, where  $L$  is the length of the cantilever (i.e., polystyrene film),  $E = 3.65$  GPa is Young's modulus of polystyrene film, and  $d$  is the width of the cantilever.

According to (1)–(3), the height tunability of the proposed RA elements is based on multiphysics, e.g., electromagnetics and mechanics. Since multiphysics simulation is difficult to perform, experimental studies are performed here in order to find the deformation tunability of the proposed RA elements. One of the fabricated elements is shown in Fig. 4. The measurement system is shown in Fig. 5. The height of the small steel patch was measured by a high-accuracy 2-D laser displacement sensor, KEYENCE LJ-G200.

Fig. 6 shows the height tunability of steel patch  $s$  with respect to input dc voltage  $V$  of electromagnet. As shown in Fig. 6(a), it is found that high applied dc voltage  $V$  is necessary to attract the steel patch to the same height  $s$  when the length of the polystyrene film  $L$  is short. The measurement results agree well with the theoretically predicted ones, except for the steep drops observed as  $s$  suddenly dropped to zero. Therefore, a long film is preferable in order to reduce the applied dc voltage. However, according to the measurement results and limitation of the size of the RA element in the  $y$ -direction at  $f = 4.4$  GHz and  $L = 40$  mm is chosen as the optimum value of  $L$ .

Fig. 6(b) shows that applied dc voltage  $V$  significantly drops if polystyrene film thickness  $t$  becomes thinner. Here, it should be noted that a paper sheet with thickness  $t = 0.1$  mm was

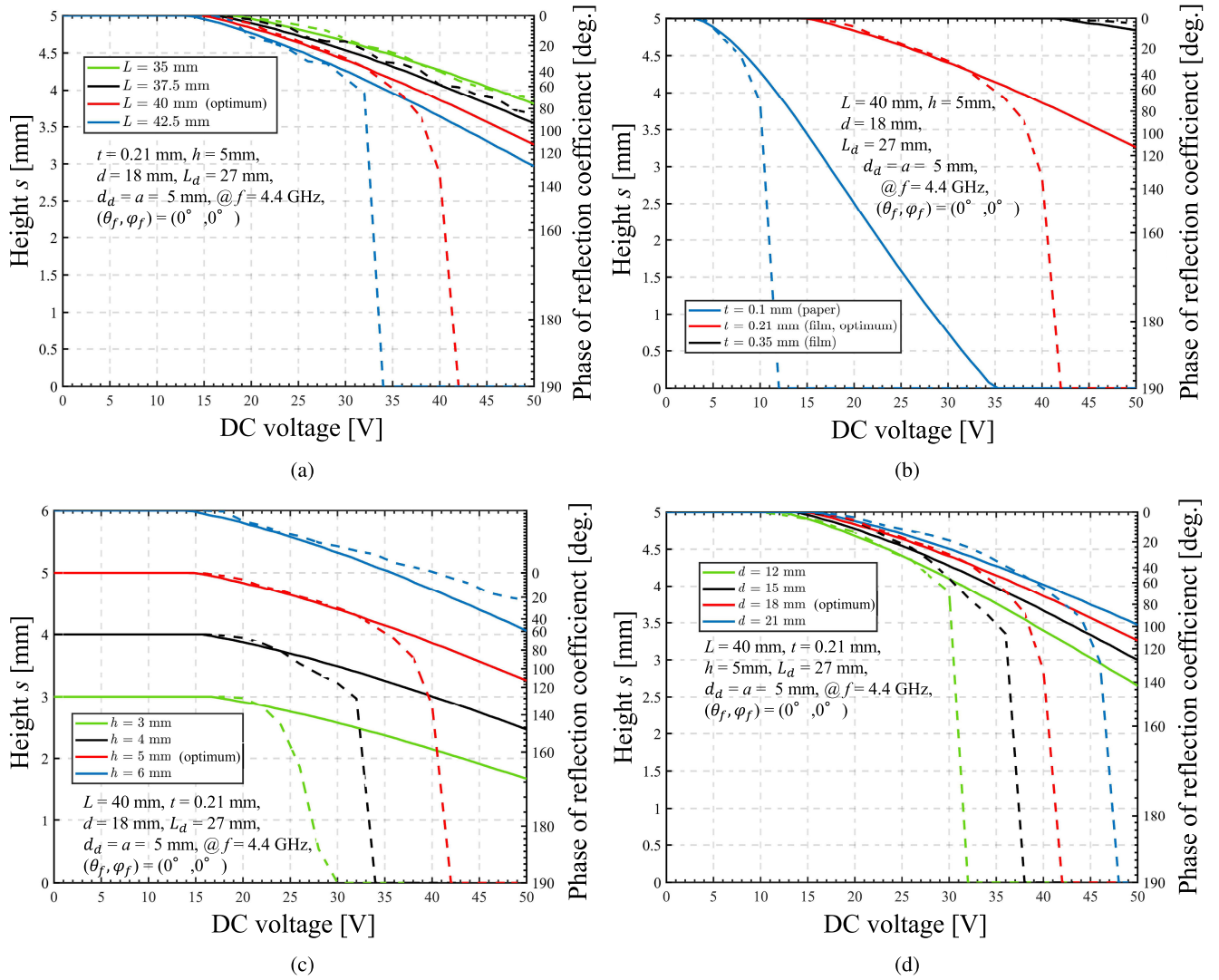


Fig. 6. Height tunability of steel patch  $s$  with respect to input dc voltage of electromagnet with different (a)  $L$ , (b)  $t$ , (c)  $h$ , and (d)  $d$  values. The solid lines are theoretical results obtained using (2) and (3) and dashed lines are measurement results. The right vertical axis shows the phase of reflection coefficient with respect to different heights  $s$ , which was shown in Fig. 2,  $\theta_f = 0$  curve.

used instead of the polystyrene film because the polystyrene film thinner than 0.21 mm was unavailable. Although thin paper is preferable to reduce the applied voltage, paper sheet is mechanically too fragile and difficult to keep flatness. Therefore, the polystyrene film with  $t = 0.21$  mm was chosen as the optimum one. Although the polystyrene film with  $t = 0.21$  mm looks fragile, it has sufficient stiffness to keep the flatness in the OFF-state once  $L$  and  $d$  are optimized. The so-called one-side clamped cantilever [38] supporting structure with trigon/rectangular blocks also contributes to keep flatness of the polystyrene film.

As shown in Fig. 6(c), relatively high applied dc voltage  $V$  is necessary for attracting the patch as the height of PLA blocks  $h$  becomes higher. On the other hand, the phase shift between ON-state and OFF-state becomes smaller than  $180^\circ$  when  $h$  becomes lower. Therefore, the level of required applied dc voltage and phase shift range are tradeoff. According to the discussion,  $h = 5$  mm is chosen as the optimum height in this work.

As shown in Fig. 6(d), the applied dc voltage  $V$  becomes lower as polystyrene film width  $d$  becomes narrower. According to the measurement results, it can be concluded that a narrower width of polystyrene film is preferred, but the mechanical stiffness of exceedingly narrow film becomes insufficient for maintaining flatness of the OFF-state RA element. Therefore,  $d = 18$  mm is chosen as the optimum width in this work.

In addition to the above discussions on the measurement results in Fig. 6(a)–(d), an interesting point should be addressed. The height of the steel patch  $s$  suddenly drops to zero as the applied dc voltage  $V$  reaches a specific threshold value. The reasons are given as follows.

The first one is the discrepancy between the fabricated RA element and its mechanical model. Equation (3) is formulated from a cantilever deflection model, where force is applied to the center of the cantilever whose edges are fixed [38]. During the formulation, it is assumed that the cantilever is uniform, the force is applied to the center

point of the cantilever, and Young's modulus  $E$  is scalar. However, in practice, the cantilever is not uniform because copper strip and steel patch are taped on the polystyrene film. Moreover, the force is applied to a specific area over the steel patch, not its center point. Also, Young's modulus  $E$  should be tensor when the mechanical anisotropy of the polystyrene film is rigorously modeled in the formulation. Such discrepancy between the fabricated RA element and its mechanical model results in a difference between theoretical formulas and measurement results.

The second one is nonlinear positive feedback, i.e., nonlinear increase of the magnetostatic force  $F$  as a function of  $s$ . According to (2), it is found that the magnetic flux density  $B$  is a nonlinear function of  $s$ . The nonlinearity of  $B$  as a function of  $s$  is also found in a datasheet of the electromagnet [36]. Therefore, the magnetostatic force  $F$  nonlinearly increases as a function of  $s$  because  $F$  is proportional to  $B^2$  as described in (1). Consequently, mechanically nonlinear positive feedback, i.e., nonlinear increase of the magnetostatic force  $F$  as  $s$  decreases, is given to the proposed element when it is ON-state. The nonlinear positive feedback results in ease of breaking the balance between the magnetostatic force and the restoring force because disturbance to the cantilever contributes to increasing the magnetostatic attracting force.

Finally, it can be concluded that the RA element is optimized mechanically at the working frequency of 4.4 GHz and 180° phase shift can be realized in the proposed design.

### III. DESIGN AND FABRICATION OF RA ANTENNA

#### A. Fabrication and Assemble of the 1-bit $25 \times 8$ RA

A 1-bit  $25 \times 8$  elements RA is fabricated to demonstrate the beam scanning ability. The fabricated RA prototype is shown in Fig. 7(a). Here, the fabricated RA prototype was designed to be large as much as possible so that it demonstrates high 1-bit resolution and superior beam scanning performance. As a result, the aperture of the fabricated prototype is rectangular, not square because the largest available aluminum ground plane was a rectangular one.

Permanent button magnets are used for tuning height of each RA element instead of the electromagnets to demonstrate the scattering performance of the proposed RA in a simple manner. UTOMAG  $12 \times 3$  mm magnet is chosen because, when this magnet is attached close against the geometrical center behind the element ground plane, the steel patch can stably bend the dipole strip downward to achieve 180° phase shift. Because the aluminum ground plane shields the backside structures from RF incident wave, electromagnets or button are isolated from the RA elements.

The RA backside view that is behind the ground plane is shown in Fig. 7(b). The 3-D-printed magnet holders, which can keep the positions of the button magnets, are placed under the ground plane. As shown in the right of Fig. 7(b), the holders can hold the button magnets individually right under the geometrical center of each element. In this work, ON/OFF-states of the RA element are controlled by whether to insert a button magnet or not in the corresponding holder.

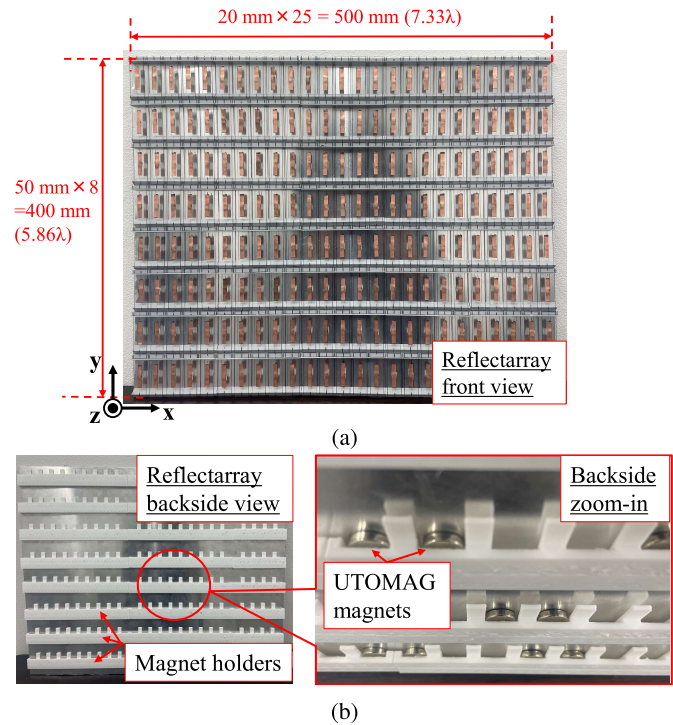


Fig. 7. Fabricated 1-bit  $25 \times 8$  (= 200) elements RA prototype: (a) front view and (b) backside view. Here,  $\lambda$  is wavelength at  $f = 4.4$  GHz.

The button magnets are inserted to the holder behind the ON-state RA elements, whereas they are not inserted to that behind the OFF-state RA elements.

Practically, installation of the automatic height tunable system of the proposed RA elements requires the development of an array of electromagnets, dc sources, and their control panel. However, this article focuses on demonstration of the RA elements using electromagnets and the development of the height tunable system is beyond the scope of this article. Therefore, the height of the RA elements in the fabricated RA prototype is tuned manually in this article.

One of the biggest problems on developing the automatic height tunable system is to reduce the power consumption of the electromagnets. The power consumption of the proposed RA mainly comes from the ON-state elements. In this work, commercial electromagnet TMB-2006T [36] was utilized, to which around 30-W prompt power should be applied in around 100  $\mu$ s for attraction of a single element. Although large power is required for bending down the element, in the mechanical measurement, it is found that only around 0.5 W is required for keeping ON-state because sufficient magnetostatic force  $F$  for keeping ON-state is available by applying low voltage  $V$  (around 4.5 V) when the height of steel patch  $s$  is small. From a systematical viewpoint, if half of the elements on the proposed RA is assumed to be kept ON-state, the estimated total power consumption for keeping the system is around 50 W. Although the power consumption of the automatic height tunable system is high compared to the conventional reconfigurable RAs, developing an efficient electromagnet or designing an element whose height can be

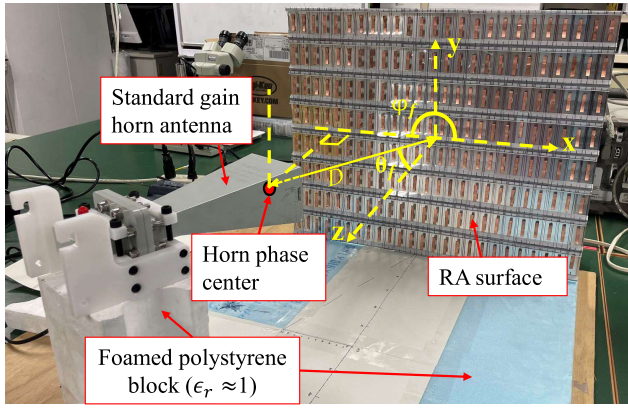


Fig. 8. Proposed RA illuminated by a horn antenna.

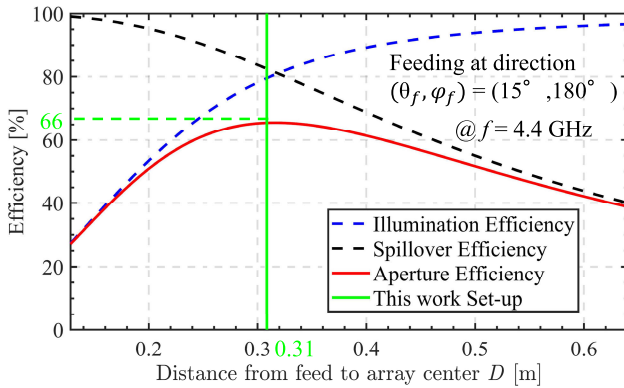


Fig. 9. Aperture efficiency of the proposed RA with respect to  $D$ .

kept without using the electromagnet is expected to reduce the power consumption. They are expected to be developed as future work.

### B. Illumination Source and RA System Optimization

Position of a primary source illuminating the proposed RA is optimized so that the aperture efficiency of the proposed RA is maximized. A primary source of the proposed RA is a standard gain horn antenna (A-INFO LB-187-10-C-SF) [39]. In order to avoid blockage by the primary source, oblique angle of incidence  $(\theta_f, \varphi_f) = (15^\circ, 180^\circ)$  is chosen. The final RA setup can be found in Fig. 8, whereas foamed polystyrene blocks ( $\epsilon_r \approx 1$ ) are used to compose the horn antenna and the proposed RA into an RA antenna system. This means that the horn is located at coordinates  $(r, \theta, \varphi) = (D, \theta_f, \varphi_f)$  in the spherical coordinate system. Simulated aperture efficiency with respect to spacing  $D$  between RA and phase center of the horn antenna is shown in Fig. 9. The aperture efficiency is expressed as follows [3]:

$$\eta_{\text{aperture}} = \eta_s \eta_i \quad (4)$$

where  $\eta_s$  is the spillover efficiency and  $\eta_i$  is the illumination efficiency. In this article,  $\eta_s$  and  $\eta_i$  are obtained in the same manner as [3] and the detailed descriptions are omitted. According to Fig. 9, it is found that the maximum aperture efficiency of 66% is achieved when  $D = 310$  mm. The illumination efficiency and the spillover efficiency corresponding to the maximum aperture efficiency are 78%

and 84%, respectively. The edge taper level of the RA corresponding to the maximum aperture efficiency is below  $-10$  dB.

Next, ON/OFF-states of the proposed RA element are designed so that the proposed RA forms a uniform phase front in a specific main-beam direction  $\hat{r}_s = (1, \theta_s, \varphi_s)$ . The ON/OFF-states of the proposed RA element are determined by the following formula [3]:

$$\Psi_i = k(R_i - \mathbf{r}_i \cdot \hat{r}_s) + \Psi_0 \quad (5)$$

where  $\Psi_i$  is the phase of reflection coefficient required for the  $i$ th element,  $k$  is the free-space wavenumber, and  $R_i$  is the distance from the primary source to the  $i$ th element.  $\mathbf{r}_i$  is a vector to represent the  $i$ th element position, and  $\hat{r}_s$  is a unit vector directed to the main-beam direction.  $\Psi_0$  is a degree of freedom on phase and is given so that the gain of the proposed RA is maximized [40]. If  $\Psi_i$  is in the range from  $0^\circ$  to  $180^\circ$ , the OFF-state ( $\Psi_{\text{off}} = 90^\circ$ ) is assigned to the  $i$ th element; otherwise, the ON-state ( $\Psi_{\text{on}} = 270^\circ$ ) is assigned to it as follows:

$$\Psi_{i(1\text{-bit})} = \begin{cases} \Psi_{\text{on}}, & 180^\circ < \Psi_i < 360^\circ \\ \Psi_{\text{off}}, & 0^\circ < \Psi_i < 180^\circ. \end{cases} \quad (6)$$

## IV. MEASUREMENT OF SCATTERING PERFORMANCE

### A. Outdoor Measurement Setup

The scattering performance of the proposed RA antenna was measured in an outdoor environment because our radio anechoic chamber is too small to measure the far field of the fabricated prototype directly. The outdoor measurement setup is shown in Fig. 10. It is well known that reflection from the ground affects the measured far field and the so-called height pattern is observed [41]. In order to eliminate the effect of the reflection from the ground, radio wave absorbers are placed at the reflection area below the midpoint between RA antenna and receiving antenna [42]. Moreover, the time-domain gating function of a vector network analyzer (VNA) is used to filter out the reflection from the ground. Due to the radio wave absorbers and the time-domain gating function, it was confirmed that the effect brought by ground plane reflection on the measured transmission coefficient is suppressed below 0.5 dB.

### B. Results of Beam Scanning Ability Validation

Gain patterns of the proposed RA antenna are shown in Fig. 11. In the results, it is found that the measured main-beam direction agrees well with those of simulated ones and the 2-D beam scanning ability of the proposed RA antenna is demonstrated. For the scenario when the RA antenna's main beam directed to the specular direction  $(15^\circ, 0)$ , the measured gain is around 22.7 dBi and the first sidelobe level is  $-13.8$  dB. Around 1-dB drop of the measured gain from the simulated one comes from material loss neglected in numerical simulation and the imperfect elimination of the reflection from the ground. As the main-beam direction of the RA antenna approaches  $\theta = 45^\circ$ , the beam starts to distort, and a grating lobe appears at around  $(\theta, \varphi) = (5^\circ, 180^\circ)$ , because

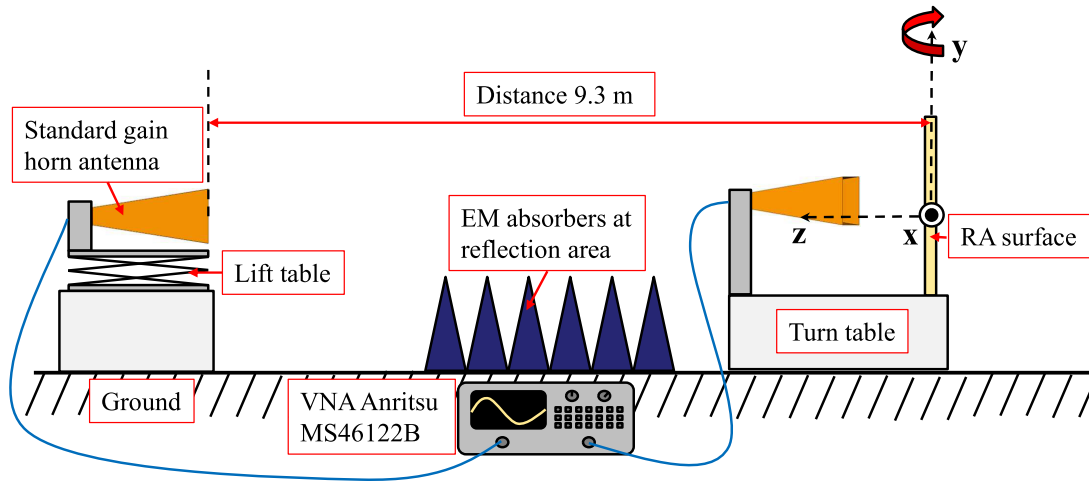


Fig. 10. Side-viewed demonstration of field experiment setup for measuring the proposed RA antenna system in an outdoor environment.

TABLE I  
GAIN LOSS BUDGET OF THE PROPOSED RA ANTENNA

Parameter	Value (dB)
Maximum directivity ( $4\pi A/\lambda^2$ )	27.3
Illumination	1.1
Spillover	0.8
1-Bit quantization	2.4
Feed blockage, phase error, material loss, out phase ground reflection, others	0.3
<b>Total loss</b>	<b>4.6</b>
<b>Gain (Aperture efficiency)</b>	<b>22.7 (34%)</b>

of the imperfect phase compensation by the 1-bit phase shift. The aperture efficiency of the RA antenna corresponding to specular reflection is 34.0%. Losses of the proposed RA are tabulated in Table I. In Table I, the illumination loss and spillover loss were obtained in Section III-B by an aperture efficiency analysis. The 1-bit quantization loss was obtained by comparing simulated gain of the proposed RA antenna with 1-bit compensated phase distribution and ideal compensated phase situation.

The frequency response of the gain and aperture efficiency of the proposed RA antenna corresponding to specular reflection was measured and the results are shown in Fig. 12(a). The bandwidth corresponding to 1-dB gain drop of the proposed RA antenna is around 410 MHz (the fractional bandwidth is 9.16%), which is comparable to the bandwidth where the 1-bit phase shift is feasible, as shown in the yellow zone of Fig. 2. According to the results, it is found that the 1-bit phase shift between the ON- and OFF-states of the proposed RA element should be kept within the operating frequency band. Otherwise, the scattering performance can be deteriorated. A frequency corresponding to the maximum gain shifts away from  $f = 4.4$  GHz because of the fabrication error or measurement misalignment.

The beam scan loss of the proposed RA antenna is shown in Fig. 12(b). For beam scanning in the  $xoz$  plane ( $\varphi_s = 0$ ), it is found that the measured gain decreases as the beam scanning angle is away from the specular direction. For example, in the scenario when the RA antenna's main beam is directed to  $(\theta_s, \varphi_s) = (45^\circ, 0)$ , the gain decreases from 22.7 to 19.5 dBi,

resulting in around 3.2-dB scan loss. The large scan loss is partially contributed by the reduction of physical aperture as the beam scanning angle increases. Imperfect 1-bit phase shift also contributes to the beam scan loss, as implied in Fig. 11(b). For beam scanning in the  $yoZ$  plane ( $\varphi_s = 90^\circ$ ), the results of Fig. 12(b) show that the gain performance significantly degrades when  $\theta_s$  is over  $20^\circ$ , e.g., scan loss of 2.9 dB at  $\theta_s = 25^\circ$  and 6.3 dB at  $\theta_s = 45^\circ$  is found. This is because the proposed element has a large spacing on the  $y$ -direction, which leads to a grating lobe problem when the RA scans to large angle.

Finally, a comparison of the proposed reconfigurable RA antenna performances with some representative reference works is summarized in Table II. Since this work is a 1-bit RA antenna system, 1-bit quantization loss is inevitable. For a fair comparison to demonstrate the high-efficiency performance of this work, most of the representative reference works shown in Table II are 1-bit RA. As a result, it is clarified that the proposed 1-bit RA achieves lower element loss and relatively high aperture efficiency over conventional ones. Besides the works shown in Table II, in the working frequency range around 5 GHz, the proposed work also exhibits distinctive element loss performance compared with electronically controlled method such as [16] and [18] (element loss around 1 dB at 5 GHz and 2.4 dB at 5.4 GHz, respectively), and mechanically controlled method such as [32] (element loss around 0.18 dB at 4.8 GHz). These reference works are also added in Table II and their quantization losses are marked as multibits. The outstanding performance of the proposed RA antenna comes from complete isolation between the RA element and the electromagnets in the RF frequency band. Therefore, it can be concluded that the proposed RA antenna is a promising technology as a high-gain and beam scanning antenna.

## V. FEASIBILITY OF THE PROPOSED RA ELEMENT AT HIGHER FREQUENCY BAND

Although the performance of the proposed RA element has been demonstrated in this study, its feasibility at the higher frequency band should be discussed, where air-fed

TABLE II  
COMPARISON OF THE PROPOSED 1-bit RA ANTENNA PERFORMANCES WITH REFERENCE WORKS

	Control method	Frequency [GHz]	Element loss [dB]	Array size [ $\lambda$ ]	Quantization loss [dB]	F/D ratio	Bandwidth (1-dB gain)	Scanning range	Aperture efficiency [%] /Gain [dBi]
[15]	P-i-n diode	60.25	4.0	114 $\times$ 114	$\sim$ 3.9	1	$\sim$ 0.8%	$\pm 20^\circ$	9.5/ 42
[16]	P-i-n diode	5.0	$<0.9$	6.6 $\times$ 6.6	$\sim$ 2.5	0.9	8.4%	$\pm 50^\circ$	15.3/ 19.2
[18]	Reverse biased diodes	5.4	2.4	3.9 $\times$ 3.3	Multi-bits	0.98	$<3.6\%$	$\pm 40^\circ$	14.0/ 13.3
[23]	Electromagnetic rotation	9.5	0.4/ 1.1	7.6 $\times$ 7.6	N.G.	0.99	9.4%	$\pm 45^\circ$	20.0/ 21.8
[24]	P-i-n diodes	11.1	1/ 2.8	3.3 $\times$ 3.3	$\sim$ 2.56	1	N.G.	$10^\circ$ to $50^\circ$	21.1/ 15.6
[30]	Mechanical rotation	10.0	$\sim 2$	13 $\times$ 13	$\sim$ 3.0	0.87	18%	0 to $60^\circ$	24.7/ 27.2
[32]	Height tuning	4.8	0.18	8.5,Circular	Multi-bits	1.3	6.2%	0 to $60^\circ$	48.6/ 25.7
<b>This work</b>	Magnetostatic force	4.4	$\sim 0.1$	7.3 $\times$ 5.9	$\sim$ 2.4	0.62	9.16%	0 to $45^\circ$	<b>34/ 22.7</b>

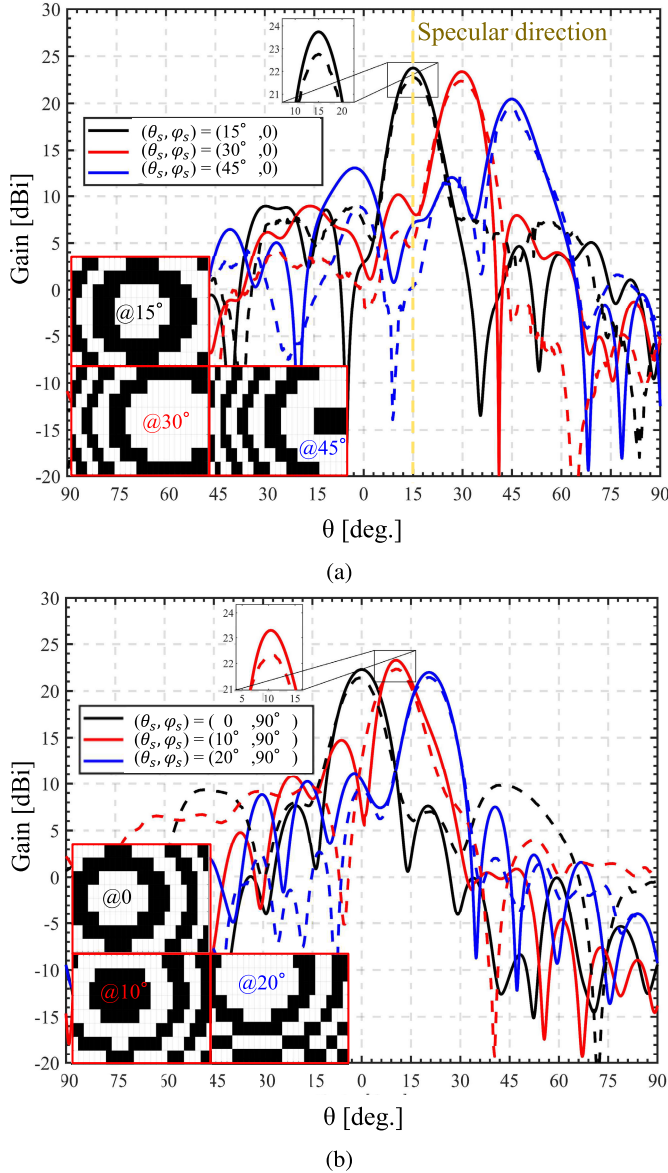


Fig. 11. Gain patterns of the proposed RA antennas at  $f = 4.4$  GHz for main beam directed in (a)  $xoz$  plane ( $\varphi_s = 0^\circ$ ) and (b)  $yo z$  plane ( $\varphi_s = 90^\circ$ ). The bold lines are simulation results obtained by FEKO, and the dashed lines are measurement results. The ON-states (white) and OFF-states (black) of the RA elements are shown in the bottom left.

antenna such as RA would exhibit distinctive advantages. Since the proposed RA element must be designed under electrical/mechanical restrictions, the operating frequency in

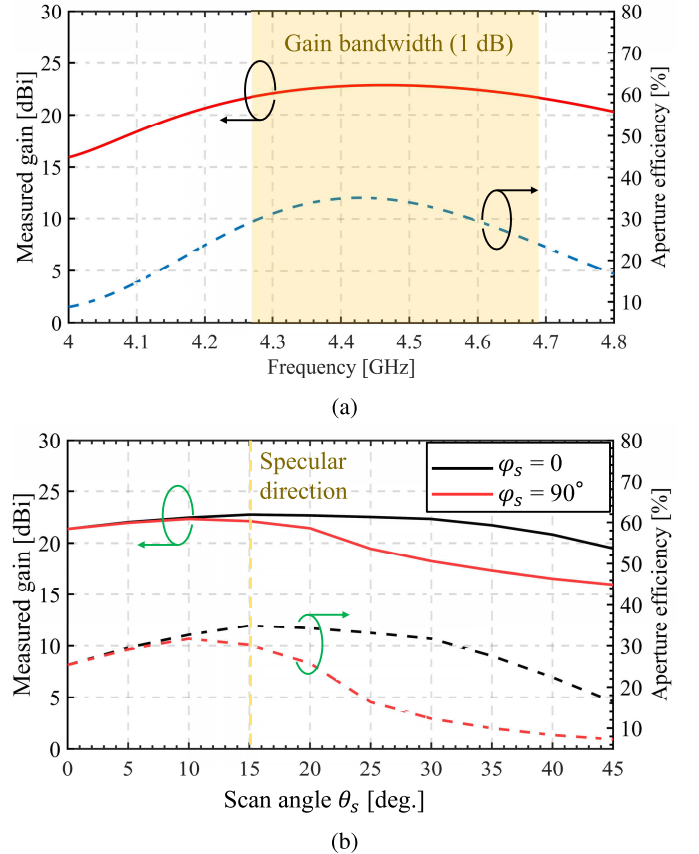


Fig. 12. Measured gain performance of the proposed RA antenna along (a) frequency band and (b) beam scanning angle in both  $xoz$  and  $yo z$  planes.

this work is only around 4.4 GHz. Here, the feasibility of the proposed RA element at the higher frequency band is discussed from the viewpoints of mechanics and electromagnetics approaches.

From the electromagnetic viewpoint, it should be demonstrated that the proposed RA element exhibits 1-bit performance at the higher frequency band without significant loss. Numerical simulation results are shown in Fig. 13. In the numerical simulation model, the element size is scaled down as frequency  $f$  changes. The phase difference of reflection coefficients between ON- and OFF-states of the RA elements is over  $166^\circ$ , ranging from 4.4 to 10 GHz. Since  $180 \pm 20^\circ$  phase tuning range is typically chosen where 1-bit reconfiguration can be sufficiently demonstrated [16], [17],  $166^\circ$  at 10 GHz is still acceptable. The reflection loss increases because the

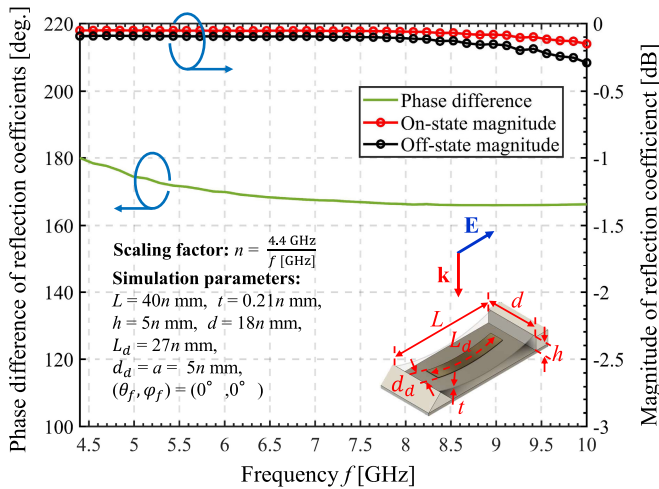


Fig. 13. Reflection performance of the proposed RA element at higher frequency band. Scaling factor  $n$  is introduced and dimensions of the RA element are scaled down as  $f$  changes.

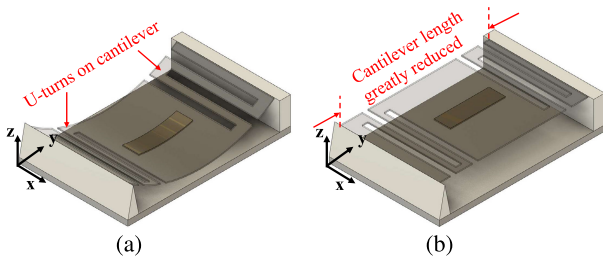


Fig. 14. Element design with reduced  $y$ -direction dimension using multiple U-turns on cantilever in (a) ON-state and (b) OFF-state.

loss tangent  $\tan\delta$  of the polystyrene film is constant during the numerical simulation, i.e., conductivity of the polystyrene film increases as the frequency  $f$  increases. The maximum reflection loss over the band is around 0.29 dB, which is a moderate value compared to conventional RA elements. According to the numerical results and discussions, it can be concluded that the 1-bit performance of the proposed RA element is achievable at the higher frequency band.

From the mechanical viewpoint, scale down of the RA element, including its mechanical system, is necessary for increasing the operating frequency. A multiple U-turns cantilever system, which is inspired by MEMS cantilever design, is a promising approach for scaling down the RA element [43]. Examples of the multiple U-turns cantilever system are shown in Fig. 14. The multiple U-turns cantilever system can save the space of the cantilever at the small expense of the flexibility of the structure. Another approach is to reduce the size of the electromagnet. To the best of authors' knowledge, the smallest available electromagnet with satisfied performance is TMN-105S [44], whose maximum diameter is around 10 mm. Application of both approaches can potentially raise the working frequency to around 8.8 GHz, which is remaining as future work.

## VI. CONCLUSION

High-efficient mechanically reconfigurable 1-bit RA elements, which can achieve isolation between RA elements and

reflection phase controlling devices using electromagnets, have been proposed. The proposed reconfigurable RA elements were composed of bendable metallic dipole over flexible supporting structures backed by a ground plane. Metallic dipole elements were attached with small steel patches and their height can be controlled using electromagnets behind the ground plane. In this way, total isolation between RA elements and RF phase shifters can be achieved. The reflection coefficient of the proposed RA element was simulated and its deformation tunability was demonstrated through theoretical and experimental analysis. A  $25 \times 8$  reconfigurable 1-bit RA antenna using the proposed element was designed and fabricated. Through an outdoor field measurement of the proposed RA antenna system, around 22.7-dBi measured gain and 34% aperture efficiency were found in a specular direction, which proved the high-efficient scattering performance of the proposed design. The element loss performance as well as aperture efficiency were very competitive in 1-bit reconfigurable RA antennas and can be a potential candidate for next-generation high-gain antenna application.

Although the performance of the proposed 1-bit RA has been demonstrated in this work, several challenging problems are still remaining: reduction of the applied dc voltage to the electromagnets, large angle beam scanning in the  $yz$  plane, and continuous height tunability (multibits). The solution to these problems is expected to further enhance the performance of the proposed RA antenna, and solving these problems is remained as future work.

## ACKNOWLEDGMENT

The authors would like to thank the staffs at the Innovation Plaza, School of Engineering, Tohoku University, Sendai, Japan, for their helpful advice.

## REFERENCES

- [1] D. Berry, R. Malech, and W. Kennedy, "The reflectarray antenna," *IEEE Trans. Antennas Propag.*, vol. AP-11, no. 6, pp. 645–651, Nov. 1963.
- [2] J. Huang, "Analysis of a microstrip reflectarray antenna for microspacecraft applications," Jet Propuls. Lab., California Inst. Technol., Nat. Aeronaut. Space Admin. (NASA), TDA Prog. Rep. 42-120, Feb. 1995, pp. 153–173.
- [3] P. Nayeri, F. Yang, and A. Z. Elsherbeni, *Reflectarray Antennas*. Hoboken, NJ, USA: Wiley, 2018.
- [4] L. Li et al., "Novel broadband planar reflectarray with parasitic dipoles for wireless communication applications," *IEEE Antennas Wireless Propag. Lett.*, vol. 8, pp. 881–885, 2009.
- [5] L. Li et al., "Frequency selective reflectarray using crossed-dipole elements with square loops for wireless communication applications," *IEEE Trans. Antennas Propag.*, vol. 59, no. 1, pp. 89–99, Jan. 2011.
- [6] K. Konno and Q. Chen, "Enhancing aperture efficiency of RA by accurately evaluating mutual coupling of reflectarray elements," *IEICE Commun. Exp.*, vol. 5, no. 9, pp. 341–346, 2016.
- [7] J. A. Encinar et al., "Dual-polarization dual-coverage reflectarray for space applications," *IEEE Trans. Antennas Propag.*, vol. 54, no. 10, pp. 2827–2837, Oct. 2006.
- [8] J. A. Encinar, M. Arrebola, L. F. de la Fuente, and G. Toso, "A transmit-receive reflectarray antenna for direct broadcast satellite applications," *IEEE Trans. Antennas Propag.*, vol. 59, no. 9, pp. 3255–3264, Sep. 2011.
- [9] P. Nayeri et al., "3D printed dielectric reflectarrays: Low-cost high-gain antennas at sub-millimeter waves," *IEEE Trans. Antennas Propag.*, vol. 62, no. 4, pp. 2000–2008, Apr. 2014.

- [10] K. Yokokawa, K. Konno, and Q. Chen, "Scattering performance of log-periodic dipole array," *IEEE Antennas Wireless Propag. Lett.*, vol. 16, pp. 740–743, 2017.
- [11] H. Ito, K. Konno, H. Sato, and Q. Chen, "Wideband scattering performance of reflectarray using log-periodic dipole array," *IEEE Antennas Wireless Propag. Lett.*, vol. 16, pp. 1305–1308, 2017.
- [12] K. Konno, H. Sato, Q. Chen, and H. Itoh, "Scattering performance of a reflectarray using log-periodic dipole array element," in *Proc. Int. Symp. Antennas Propag. (ISAP)*, Oct. 2017, pp. 1–2.
- [13] K. Konno, Q. Yuan, and Q. Chen, "Ninja array antenna: Novel approach for low backscattering phased array antenna," *IET Microw., Antennas Propag.*, vol. 12, no. 3, pp. 346–353, Feb. 2018.
- [14] K. Konno, Q. Chen, and Q. Yuan, "Scattering and radiation performance of Ninja array antennas," in *Proc. APMC*, Nov. 2018, pp. 1–3.
- [15] H. Kamoda, T. Iwasaki, J. Tsumochi, T. Kuki, and O. Hashimoto, "60-GHz electronically reconfigurable large reflectarray using single-bit phase shifters," *IEEE Trans. Antennas Propag.*, vol. 59, no. 7, pp. 2524–2531, Jul. 2011.
- [16] J. Han, L. Li, G. Liu, Z. Wu, and Y. Shi, "A wideband 1 bit  $12 \times 12$  reconfigurable beam-scanning reflectarray: Design, fabrication, and measurement," *IEEE Antennas Wireless Propag. Lett.*, vol. 18, no. 6, pp. 1268–1272, Jun. 2019, doi: [10.1109/LAWP.2019.2914399](https://doi.org/10.1109/LAWP.2019.2914399).
- [17] W. Wu, K.-D. Xu, Q. Chen, T. Tanaka, M. Kozai, and H. Minami, "A wideband reflectarray based on single-layer magneto-electric dipole elements with 1-bit switching mode," *IEEE Trans. Antennas Propag.*, vol. 70, no. 12, pp. 12346–12351, Dec. 2022, doi: [10.1109/TAP.2022.3209693](https://doi.org/10.1109/TAP.2022.3209693).
- [18] M. Riel and J.-J. Laurin, "Design of an electronically beam scanning reflectarray using aperture-coupled elements," *IEEE Trans. Antennas Propag.*, vol. 55, no. 5, pp. 1260–1266, May 2007, doi: [10.1109/TAP.2007.895586](https://doi.org/10.1109/TAP.2007.895586).
- [19] F. Venneri, S. Costanzo, and G. Di Massa, "Design and validation of a reconfigurable single varactor-tuned reflectarray," *IEEE Trans. Antennas Propag.*, vol. 61, no. 2, pp. 635–645, Feb. 2013.
- [20] T. Makdissy, R. Gillard, E. Fourn, E. Girard, and H. Legay, "Phase-shifting cell loaded with variable capacitances for dual linearly polarised reflectarrays," *Electron. Lett.*, vol. 48, no. 21, pp. 1319–1320, Oct. 2012.
- [21] T. Makdissy, R. Gillard, E. Fourn, E. Girard, and H. Legay, "Phase-shifting cell for dual linearly polarized reflectarrays with reconfigurable potentialities," *IEEE Antennas Wireless Propag. Lett.*, vol. 13, pp. 11–14, 2014.
- [22] H. Yang, F. Yang, S. Xu, M. Li, X. Cao, and J. Gao, "A 1-bit multipolarization reflectarray element for reconfigurable large-aperture antennas," *IEEE Antennas Wireless Propag. Lett.*, vol. 16, pp. 581–584, 2017.
- [23] F. Wu, R. Lu, J. Wang, Z. H. Jiang, W. Hong, and K.-M. Luk, "A circularly polarized 1 bit electronically reconfigurable reflectarray based on electromagnetic element rotation," *IEEE Trans. Antennas Propag.*, vol. 69, no. 9, pp. 5585–5595, Sep. 2021, doi: [10.1109/TAP.2021.3069551](https://doi.org/10.1109/TAP.2021.3069551).
- [24] X. Cao, Q. Chen, T. Tanaka, M. Kozai, and H. Minami, "A 1-bit time-modulated reflectarray for reconfigurable-intelligent-surface applications," *IEEE Trans. Antennas Propag.*, vol. 71, no. 3, pp. 2396–2408, Mar. 2023, doi: [10.1109/TAP.2022.3233659](https://doi.org/10.1109/TAP.2022.3233659).
- [25] R. L. Haupt and M. Lanagan, "Reconfigurable antennas," *IEEE Antennas Propag. Mag.*, vol. 55, no. 1, pp. 49–61, Feb. 2013.
- [26] A. C. Polycarpou, M. A. Christou, and N. C. Papanicolaou, "Tunable patch antenna printed on a biased nematic liquid crystal cell," *IEEE Trans. Antennas Propag.*, vol. 62, no. 10, pp. 4980–4987, Oct. 2014.
- [27] M. R. Chaharmir, I. Shaker, M. Cuhaci, and A. Sebak, "Mechanically controlled reflectarray antenna for beam switching and beam shaping in millimetre-wave applications," *Electron. Lett.*, vol. 39, no. 7, pp. 591–592, Apr. 2003.
- [28] V. F. Fusco, "Mechanical beam scanning reflectarray," *IEEE Trans. Antennas Propag.*, vol. 53, no. 11, pp. 3842–3844, Nov. 2005.
- [29] V. Srinivasan and V. F. Fusco, "Circularly polarised mechanically steerable reflectarray," *IEE Proc. Microw. Antennas Propag.*, vol. 152, no. 6, pp. 511–514, Dec. 2005.
- [30] M. Wang, Y. Mo, W. Xie, N. Hu, Z. Chen, and Z. Tian, "A 1-Bit all-metal wide-angle and multipolarization beam-scanning reconfigurable reflectarray antenna," *IEEE Antennas Wireless Propag. Lett.*, vol. 22, no. 5, pp. 1015–1019, May 2023, doi: [10.1109/LAWP.2022.3230751](https://doi.org/10.1109/LAWP.2022.3230751).
- [31] X. Yang et al., "A broadband high-efficiency reconfigurable reflectarray antenna using mechanically rotational elements," *IEEE Trans. Antennas Propag.*, vol. 65, no. 8, pp. 3959–3966, Aug. 2017.
- [32] X. Yang et al., "A mechanically reconfigurable reflectarray with slotted patches of tunable height," *IEEE Antennas Wireless Propag. Lett.*, vol. 17, no. 4, pp. 555–558, Apr. 2018.
- [33] G.-B. Wu, S.-W. Qu, and S. Yang, "Wide-angle beam-scanning reflectarray with mechanical steering," *IEEE Trans. Antennas Propag.*, vol. 66, no. 1, pp. 172–181, Jan. 2018.
- [34] M. I. Abbasi, M. H. Dahri, M. H. Jamaluddin, N. Seman, M. R. Kamarudin, and N. H. Sulaiman, "Millimeter wave beam steering reflectarray antenna based on mechanical rotation of array," *IEEE Access*, vol. 7, pp. 145685–145691, 2019.
- [35] S. V. Hum and J. Perruisseau-Carrier, "Reconfigurable reflectarrays and array lenses for dynamic antenna beam control: A review," *IEEE Trans. Antennas Propag.*, vol. 62, no. 1, pp. 183–198, Jan. 2014, doi: [10.1109/TAP.2013.2287296](https://doi.org/10.1109/TAP.2013.2287296).
- [36] *TESLA TMB-2006T Datasheet*. Accessed: Sep. 5, 2023. [Online]. Available: <https://www.teslanet.co.jp/wp-content/uploads/2018/03/TMB-2006T.pdf>
- [37] N. Ida, *Engineering Electromagnetics*, 3rd ed. New York, NY, USA: Springer-Verlag, 2015, ch. 9.
- [38] *MiSUMi Technical Data, Calculation of Beam Deflection*. Accessed: Sep. 5, 2023. [Online]. Available: <https://us.misumi-ec.com/pdf/tech/mold/p1707.pdf>
- [39] *A-Info Technical Specification, LB-187-10 Data sheet*. Accessed: Sep. 5, 2023. [Online]. Available: [http://www.ainfoinc.com.cn/en/pro\\_pdf/new\\_products/antenna/Standard%20Gain%20Horn%20Antenna/t\\_LB-187-10.pdf](http://www.ainfoinc.com.cn/en/pro_pdf/new_products/antenna/Standard%20Gain%20Horn%20Antenna/t_LB-187-10.pdf)
- [40] H. Yang et al., "A 1-bit  $10 \times 10$  reconfigurable reflectarray antenna: Design, optimization, and experiment," *IEEE Trans. Antennas Propag.*, vol. 64, no. 6, pp. 2246–2254, Jun. 2016, doi: [10.1109/TAP.2016.2550178](https://doi.org/10.1109/TAP.2016.2550178).
- [41] R. Lytle, "Ground reflection effects upon radiated and received signals as viewed via image theory," *IEEE Trans. Antennas Propag.*, vol. AP-20, no. 6, pp. 736–741, Nov. 1972, doi: [10.1109/TAP.1972.1140328](https://doi.org/10.1109/TAP.1972.1140328).
- [42] F. Saccardi, F. Mioc, A. Giacomini, and L. J. Foged, "Estimation of the realistic ground effect in free-space automotive measurements," in *Proc. AMTA*, Williamsburg, VA, USA, 2018, pp. 1–5.
- [43] F. Chollet and H. Liu. (2012). *A (Not So) Short Introduction to MEMS*. version 5.0. [Online]. Available: <http://memscyclopedia.org/introMEMS.html>
- [44] *TESLA TMB-105S Datasheet*. Accessed: Sep. 5, 2023. [Online]. Available: <https://www.teslanet.co.jp/pdf/small-electromagnets.pdf>



**Ao Hu** (Graduate Student Member, IEEE) received the B.E. degree from the Huazhong University of Science and Technology, Wuhan, China, in 2018, and the M.Sc. degree from the KTH Royal Institute of Technology, Stockholm, Sweden, in 2019. He is currently pursuing the Ph.D. degree with Tohoku University, Sendai, Japan.

He is also a Student Member with the AIE-WISE Program for AI Electronics, Tohoku University. His research interests include mechanically actuated reflectarray antennas and reconfigurable intelligent surfaces.



**Keisuke Konno** (Member, IEEE) received the B.E., M.E., and D.E. degrees from Tohoku University, Sendai, Japan, in 2007, 2009, and 2012, respectively.

Since 2012, he has been with the Department of Communications Engineering, Graduate School of Engineering, Tohoku University, where he is currently an Associate Professor. He was a Visiting Scholar with the ElectroScience Laboratory, The Ohio State University, Columbus, OH, USA, from 2015 to 2017. His research interests include

computational electromagnetics, array antennas, reflectarrays, and source reconstruction.

Dr. Konno is a member of IEICE. He received the Encouragement Award for Young Researcher and Most Frequent Presentations Award from the Technical Committee on Antennas and Propagation of Japan in 2010, the Young Researchers Award from the Institute of Electronics, Information and Communication Engineers (IEICE) of Japan in 2011, the IEEE EMC Society Sendai Chapter Student Brush-up Session and EMC Sendai Seminar Student Best Presentation Award in 2011, the JSPS Washington Director Award in 2016, the MHz Rectenna Award in 2017, the Young Researchers Award for ECEI of Tohoku University in 2018, the Minoru Ishida Award in 2018, the IEEE AP-S Japan Young Engineer Award in 2018, the TOKIN Foundation Research Encouragement Award in 2019, the IEICE Communications Society Distinguished Contributions Award in 2019, and the JSPS Postdoctoral Fellowships for Research Abroad.



**Qiang Chen** (Senior Member, IEEE) received the B.E. degree from Xidian University, Xi'an, China, in 1986, and the M.E. and D.E. degrees from Tohoku University, Sendai, Japan, in 1991 and 1994, respectively.

He is currently an Associate Professor with the Department of Communications Engineering, Tohoku University. His primary research interests include computational electromagnetics, array antennas, and antenna measurement.

Dr. Chen is a member of the Institute of Electronics, Information and Communication Engineers (IEICE). He received

the Young Scientists Award in 1993 and the Best Paper Award and Zen-ichi Kiyasu Award in 2009 from the Institute of Electronics, Information and Communication Engineers (IEICE) of Japan. He was the Secretary and the Treasurer of the IEEE Antennas and Propagation Society Japan Chapter in 1998, the Secretary of the Technical Committee on Electromagnetic Compatibility of IEICE from 2004 to 2006, and the Technical Committee on Antennas and Propagation of IEICE from 2008 to 2010, and an Associate Editor of *IEICE Transactions on Communications* from 2007 to 2012. He is the Chair of the IEICE Technical Committee on Photonics-Applied Electromagnetic Measurement.



**Toru Takahashi** (Senior Member, IEEE) was born in Kanagawa, Japan, in January 1970. He received the B.E. and M.E. degrees in electrical engineering and the D.E. degree from Waseda University, Tokyo, Japan, in 1992, 1994, and 2010, respectively.

In 1994, he joined Mitsubishi Electric Corporation, Kamakura, Japan, where he has been engaged in research and development on antennas, radar systems, and radio communication systems. He is currently the Manager of the Antennas Technology Department, Information Technology Research and

Development Center, Mitsubishi Electric Corporation.

Dr. Takahashi is a Senior Member of the Institute of Electronics, Information and Communication Engineers (IEICE) of Japan. He received the Young Engineer Award from IEICE of Japan in 1999 and the IEICE Communications Society Best Paper Award in 2013 and 2018.